PHYSICS OF FLUIDS **26**, 057101 (2014)

Rarefied gas flow in a rectangular enclosure induced by non-isothermal walls

Manuel Vargas,[1] Giorgos Tatsios,[1] Dimitris Valougeorgis,[1,a)]
and Stefan Stefanov[2]
[1]*Department of Mechanical Engineering, University of Thessaly, 38334 Volos, Greece*
[2]*Institute of Mechanics, Bulgarian Academy of Sciences, Sofia, Bulgaria*

(Received 29 January 2014; accepted 23 April 2014; published online 20 May 2014)

The flow of a rarefied gas in a rectangular enclosure due to the non-isothermal walls with no synergetic contributions from external force fields is investigated. The top and bottom walls are maintained at constant but different temperatures and along the lateral walls a linear temperature profile is assumed. Modeling is based on the direct numerical solution of the Shakhov kinetic equation and the Direct Simulation Monte Carlo (DSMC) method. Solving the problem both deterministically and stochastically allows a systematic comparison and verification of the results as well as the exploitation of the numerical advantages of each approach in the investigation of the involved flow and heat transfer phenomena. The thermally induced flow is simulated in terms of three dimensionless parameters characterizing the problem, namely, the reference Knudsen number, the temperature ratio of the bottom over the top plates, and the enclosure aspect ratio. Their effect on the flow configuration and bulk quantities is thoroughly examined. Along the side walls, the gas flows at small Knudsen numbers from cold-to-hot, while as the Knudsen number is increased the gas flows from hot-to-cold and the thermally induced flow configuration becomes more complex. These flow patterns with the hot-to-cold flow to be extended to the whole length of the non-isothermal side walls may exist even at small temperature differences and then, they are enhanced as the temperature difference between the top and bottom plates is increased. The cavity aspect ratio also influences this flow configuration and the hot-to-cold flow is becoming more dominant as the depth compared to the width of the cavity is increased. To further analyze the flow patterns a novel solution decomposition into ballistic and collision parts is introduced. This is achieved by accordingly modifying the indexing process of the typical DSMC algorithm. The contribution of each part of the solution is separately examined and a physical interpretation of the flow configuration, including the hot-to-cold flow close to the side walls, in the whole range of the Knudsen number is provided. [http://dx.doi.org/10.1063/1.4875235]

I. INTRODUCTION

Thermally induced non-equilibrium gas flows in cavities have lately received considerable attention. At some extent this is due to the potential implementation of such flows in the emerging field of microfluidics[1] and more specifically in vacuum packaged MEMS[2,3] as well as in micropumps,[4,5] and microactuators/microsensors.[6,7] In addition to that, over the years, temperature driven flows in cavities have been commonly applied in rarefied gas dynamics as prototype problems in order to investigate theoretically interesting physical phenomena[8–12] as well as to benchmark and validate novel numerical schemes.[13–15]

[a)]Author to whom correspondence should be addressed. Electronic mail: diva@mie.uth.gr

The extent to which the gas flow departs from local thermodynamic equilibrium is defined by the Knudsen number, which is the ratio of the mean free path of a gas molecule over a characteristic length of the flow. Gas flows in the slip and early transition regimes may be treated with the conventional Navier-Stokes-Fourier (NSF) analysis subject to slip and jump boundary conditions,[16] as well as with higher order continuum models.[17] Gas flows in the transition and free molecular regimes must be described by kinetic theory,[18,19] which is certainly valid in the whole range of the Knudsen number but in the slip regime compared to the extended hydrodynamics theory is computationally more expensive.

The literature survey on rarefied gas flows driven by temperature differences on the basis of kinetic theory is very extensive. A thorough description of various types of thermal flows, including the thermal creep flow, thermal stress slip flow, and nonlinear thermal stress flow in various configurations may be found in the recent book by Sone.[20] Here, we are focusing solely to rarefied gas flows in enclosures driven by non-isothermal walls with no synergetic contributions from external force fields.

The flow generated by thermal creep in a rectangular enclosure for zero-gravity conditions was investigated by the Direct Simulation Monte Carlo (DSMC) method in Ref. 21. The top and bottom walls were kept at different temperatures and along the side walls a linear temperature profile was assumed. Two main counter-rotating vortices have been observed with mass flow, as expected, from cold to hot in the vicinity of the side walls. The gas flow in a square container, where the left and right halves of the container wall were maintained at uniform but different temperature, has been also considered[8] by numerically solving the Bhatnagar-Gross-Krook (BGK) equation. In that discontinuous wall temperature configuration, the basic flow mechanism is the same as in the thermal creep flow but this flow in the continuum limit, contrary to the thermal creep flow, vanishes in a non-uniform manner. A study on the importance of the imposed boundary conditions in steady highly rarefied gas flows induced by non-uniform wall temperature has been recently carried out on the basis of the Boltzmann equation and the DSMC method.[22] It has been deduced that by applying the Cercignani-Lampis (CL) gas-surface interaction model[23] a steady flow is induced even in the free molecular limit, while as it is known from earlier theoretical investigations in this limit and for Maxwell-type boundary conditions the flow velocity is vanishing.[11] Complimentary work with the Lord model[24] has shown that no steady flow is induced as in the case of the Maxwell model.

In order to model vacuum packaged MEMS, the flow and heat transfer in an enclosure with a hot surface in the bottom has been simulated by the DSMC method in Ref. 3. The effect of the temperature gradient and of the temperature discontinuities is examined and it is deduced that when the bottom temperature is partly uniform only close to the center of the bottom plate, the gas flow is enhanced due to thermal creep and as a result the heat transfer in the hot chip bottom surface is also enhanced. The reported rarefied flow close to the wall is according to the typical thermal creep mechanism[20] from cold to hot.

Similar studies of the heat transfer through rarefied gases confined in microcavities have been reported in Refs. 14 and 15. In the former work[14] it has been demonstrated that the regularized-13 (R13) equations[25] result to a numerical method which is applicable in the slip and early transition regime capturing flow characteristics and features which are well beyond the NSF range. In the latter work[15] it has been shown that the unified gas-kinetic scheme[26] is indeed a reliable and accurate flow solver for low-speed non-equilibrium flows. Interestingly, in both works it has been observed that the gas flow close to the wall is not necessarily going from the cold to the hot wall region. Depending on the flow parameters the flow along the boundary may move from hot to cold regions as well. In both works this unexpected flow pattern has been also confirmed by DSMC simulations. According to Ref. 14 this flow behavior is due to the opposite contribution of the viscous and transpirational parts of the tangential velocity at the side walls, which are caused by the shear stress and the tangential heat flux, respectively.

Based on all above it is evident that thermally induced rarefied gas flows in enclosures although geometrically are relatively simple flow configurations, they still are rich in non-equilibrium physical phenomena. Therefore, despite the work performed and the progress achieved, it still remains a topic of major theoretical, computational, and practical importance and further investigation will be valuable.

In the present work, the thermally induced flow in a two-dimensional rectangular enclosure with constant temperature gradients along the lateral walls is investigated in a wide range of the Knudsen number covering the slip and transitions regimes and for small, moderate, and large temperature differences between the bottom and the top walls. Boundary conditions with purely diffuse accommodation are considered. Various enclosure aspect ratios are simulated. Modeling is based on the numerical solution of the Shakhov kinetic model[27,28] and the DSMC method.[19] Solving the problem both deterministically and stochastically allows a systematic comparison and verification of the results and more important the exploitation of the advantages of each approach in the numerical investigation of the flow and heat transfer patterns. The influence of the Knudsen number, the temperature ratio, and the cavity aspect ratio on the bulk quantities is examined. Depending on the flow in addition to the well-known thermal creep flow, the recently reported flow pattern from hot-to-cold in the vicinity of the non-isothermal wall is observed. Furthermore, based on the DSMC procedure, the solution is decomposed into the so-called ballistic and collision parts and the contribution of each part to the structure of the flow is studied in order to explain the flow behavior along the lateral walls. The methodology to achieve that, as far as the authors are aware of, is presented for first time in the literature.

II. FLOW CONFIGURATION AND DEFINITION OF PARAMETERS

A monatomic rarefied gas is contained in a two-dimensional enclosure with rectangular cross section $W \times H$. The orthogonal cross section of the enclosure and the origin of the coordinate system are shown in Fig. 1. The bottom and top boundaries at $y' = 0$ and $y' = H$ are kept isothermal at temperatures T_H and T_C with $T_C < T_H$, while along the side boundaries at $x' = \pm W/2$ a linear temperature profile is assumed according to $T_S = T_H - (T_H - T_C)y'/H$. The enclosure is considered as unbounded in the third direction and end effects in that direction are neglected, while radiation and gravity effects are also assumed to be negligible. The gas-surface interaction is taken to be purely diffusive to all four boundaries.

In view of the above set-up, a symmetric about $x' = 0$ thermal creep type flow of the rarefied gas is expected. In the vicinity of the two lateral walls at $x' = \pm W/2$ there will be a mass flow in the negative y direction from cold to hot and due to mass conservation a mass flow of comparable magnitude does arise near the symmetry axis $x' = 0$. The presence of the non-isothermal side walls forces the thermal creep driven gas into a circulatory motion creating two counter-rotating vortices. This flow pattern, shown in Fig. 1(a), has been captured in Ref. 21 for a square enclosure and for small Knudsen numbers. The vortices of this flow pattern are named Vortex-type I.

Recent work[29] however, has revealed that in the same set-up, with the specific temperature ratio of $T_C/T_H = 0.1$, when the Knudsen number is adequately large additional vortices in the two bottom corners may appear and as the Knudsen number is increased they are further increased.

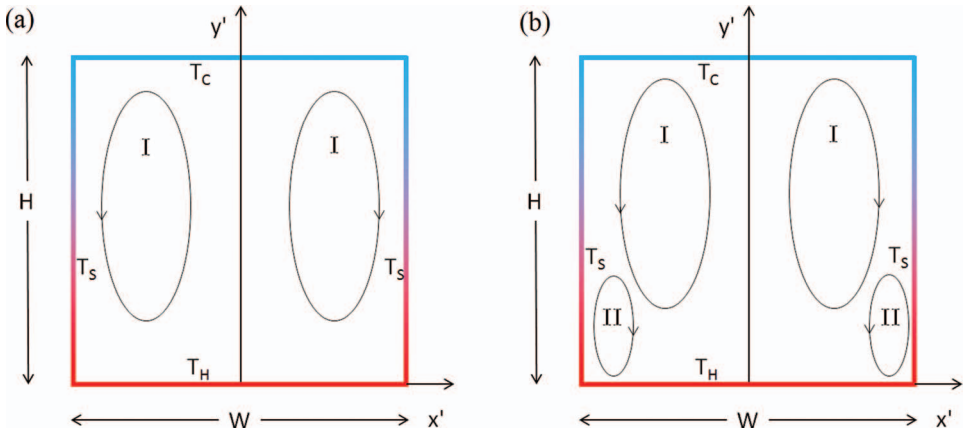

FIG. 1. View of the non-isothermal wall enclosure and flow pattern with (a) Vortex-type I and (b) with Vortex-types I and II.

These vortices are counter rotating to the main ones, i.e., the gas flows from hot-to-cold along the lateral walls. Now, the flow pattern, shown in Fig. 1(b), consists of four eddies, namely, two eddies of type I, which are squeezed towards the center and the top of the cavity and two additional vortices named, Vortex-type II, which are rotating along the lateral walls in the cold-to-hot direction. It is noted that we refer to these two types of vortices as I and II, instead of using the typical terminology of primary and secondary vortices, because as it will be seen, depending upon the flow parameters may both occupy small or large regions of the flow domain and may both become important in the characterization of the flow pattern. As it has been pointed in Sec. I, similar observations in enclosures with a slightly different non-isothermal wall set-up have been reported in Refs. 14 and 15.

Here, the flow configuration described above (Fig. 1) is computationally investigated in a detailed and systematic manner based on kinetic theory principles. The macroscopic quantities of interest include the number density distribution $N(x', y')$, the two component velocity vector $\boldsymbol{U} = \left[U_x\left(x', y'\right), U_y\left(x', y'\right)\right]$, the shear stress tensor $P_{xy}(x', y')$, the temperature distribution $T(x', y')$, and the two component heat flux vector $\boldsymbol{Q} = \left[Q_x\left(x', y'\right), Q_y\left(x', y'\right)\right]$, while the gas pressure is given by $P = Nk_BT$.

The solution is determined by three main dimensionless parameters, namely, the reference Knudsen number defined as

$$Kn_0 = \frac{\sqrt{\pi}}{2}\frac{\mu_0 \upsilon_0}{P_0 W}, \tag{1}$$

the temperature ratio T_C/T_H, and the aspect ratio of the two-dimensional cavity H/W. In Eq. (1), P_0 is a reference pressure, W is the width of the cavity, which is taken as the characteristic length, μ_0 is the gas viscosity at reference temperature T_0, and $\upsilon_0 = \sqrt{2k_BT_0/m}$, with k_B and m denoting the Boltzmann constant and the gas molecular mass, respectively, is the most probable molecular velocity, which is taken as the characteristic velocity. The reference number density N_0 is related to the reference pressure and temperature according to $P_0 = N_0k_BT_0$. Then, it is convenient to introduce the dimensionless quantities:

$$\begin{aligned} &x = x'/W \quad y = y'/W, \\ &n = N/N_0, \quad u_x = U_x/\upsilon_0, \quad u_y = U_y/\upsilon_0, \quad p = P/P_0, \quad \tau = T/T_0, \\ &q_x = Q_x/\left(P_0\upsilon_0\right), \quad q_y = Q_y/\left(P_0\upsilon_0\right). \end{aligned} \tag{2}$$

It is noted that $x \in [-1/2, 1/2]$ and $y \in [0, H/W]$ are the space variables, while n, (u_x, u_y), p, τ, with $p = n \times \tau$ and (q_x, q_y) are the two-dimensional distributions of the number density, the two components of the velocity vector, the gas pressure and temperature, and the two components of the heat flux vector, respectively. Then, to proceed with the mathematical manipulation, the molecular interaction must be specified. The Inverse Power Law (IPL) interaction,[19] is introduced yielding a viscosity of the form $\mu = \mu_0\tau^{\omega}$, with the parameter $\omega \in [1/2, 1]$. The values of $\omega = 1/2$ and $\omega = 1$ correspond to the limiting cases of hard sphere and Maxwell molecules.

The solution of the problem described above is obtained in a deterministic manner by numerically solving the nonlinear Shakhov model equations and in a stochastic manner by the DSMC method presented in Secs. III and IV, respectively.

III. DETERMINISTIC KINETIC MODELING

In kinetic modeling the main unknown is the distribution function, which for this flow configuration is a function of five independent variables: the two space variables (x', y') and the three components of the molecular velocity vector $\boldsymbol{\xi} = \left(\xi_x, \xi_y, \xi_z\right)$, i.e., $f = f\left(x', y', \boldsymbol{\xi}\right)$. The flow is simulated by the nonlinear Shakhov kinetic model,[27,28] which has been proved to be a reliable model for non-isothermal flows,[30–34] subject to purely diffuse boundary conditions. In the course of this work the deterministic solution has been proved always very reliable including the cases of small temperature differences and large Knudsen numbers, both characterized by very low velocity

speeds. The formulation of the governing equations and the implemented numerical scheme are provided in Secs. III A and III B, respectively.

A. Formulation of the Shakhov kinetic model

The nonlinear Shakhov model for the steady-state two-dimensional flow under consideration takes the form

$$\xi_x \frac{\partial f}{\partial x'} + \xi_y \frac{\partial f}{\partial y'} = \frac{P}{\mu}(f^S - f), \tag{3}$$

where P is the local pressure, $\mu = \mu(T)$ is the viscosity at local temperature T, and

$$f^S = f^M \left[1 + \frac{2}{15}\frac{m}{N(k_B T)^2}\left[Q_x(\xi_x - U_x) + Q_y(\xi_y - U_y)\right] \times \left(\frac{m}{2k_B T}\left[(\xi_x - U_x)^2 + (\xi_y - U_y)^2 + \xi_z^2\right] - \frac{5}{2}\right)\right] \tag{4}$$

with

$$f^M = \frac{N}{(2\pi RT)^{3/2}} \exp\left[-\frac{m}{2k_B T}\left[(\xi_x - U_x)^2 + (\xi_y - U_y)^2 + \xi_z^2\right]\right] \tag{5}$$

being the local Maxwellian. The dimensionless distribution function $g = f\upsilon_0^3/N_0$ and molecular velocity $\boldsymbol{\zeta} = \boldsymbol{\xi}/\upsilon_0$, along with the reference Knudsen number defined by Eq. (1) and the dimensionless quantities defined by Eq. (2), are introduced into Eqs. (3)–(5) to yield after some straightforward manipulation the corresponding equations in dimensionless form:

$$\zeta_x \frac{\partial g}{\partial x} + \zeta_y \frac{\partial g}{\partial y} = \frac{1}{Kn_0}\frac{\sqrt{\pi}}{2} n\tau^{1-\omega}\left(g^S - g\right), \tag{6}$$

$$g^S = g^M\left(1 + \frac{4}{15}\frac{1}{n\tau^2}\left[q_x(\zeta_x - u_x) + q_y(\zeta_y - u_y)\right]\left[\frac{(\zeta_x - u_x)^2 + (\zeta_y - u_y)^2 + \zeta_z^2}{\tau} - \frac{5}{2}\right]\right), \tag{7}$$

$$g^M = \frac{n}{(\pi\tau)^{3/2}} \exp\left[-\frac{(\zeta_x - u_x)^2 + (\zeta_y - u_y)^2 + \zeta_z^2}{\tau}\right]. \tag{8}$$

The IPL molecular interaction has been introduced in the derivation of Eqs. (6)–(8).

Furthermore, taking advantage of the two-dimensionality of the problem, the ζ_z component of the molecular velocity can be eliminated by introducing the reduced distribution functions $\varphi = \int_{-\infty}^{\infty} g d\zeta_z$ and $\psi = \int_{-\infty}^{\infty} \zeta_z^2 g d\zeta_z$. By operating accordingly on Eqs. (6)–(8), the following two coupled integro-differential equations for the unknown reduced distribution functions $\varphi = \varphi(x, y, \zeta_x, \zeta_y)$ and $\psi = \psi(x, y, \zeta_x, \zeta_y)$ are obtained:

$$\zeta_x \frac{\partial \varphi}{\partial x} + \zeta_y \frac{\partial \varphi}{\partial y} = \frac{1}{Kn_0}\frac{\sqrt{\pi}}{2} n\tau^{1-\omega}\left(\varphi^S - \varphi\right). \tag{9}$$

$$\zeta_x \frac{\partial \psi}{\partial x} + \zeta_y \frac{\partial \psi}{\partial y} = \frac{1}{Kn_0}\frac{\sqrt{\pi}}{2} n\tau^{1-\omega}\left(\psi^S - \psi\right). \tag{10}$$

Here,

$$\varphi^S = \varphi^M \left(1 + \frac{4}{15}\frac{1}{n\tau^2}\left[q_x\left(\zeta_x - u_x\right) + q_y\left(\zeta_y - u_y\right)\right]\left[\frac{\left(\zeta_x - u_x\right)^2 + \left(\zeta_y - u_y\right)^2}{\tau} - 2\right]\right), \quad (11)$$

$$\psi^S = \psi^M \left(1 + \frac{4}{15}\frac{1}{n\tau^2}\left[q_x\left(\zeta_x - u_x\right) + q_y\left(\zeta_y - u_y\right)\right]\left[\frac{\left(\zeta_x - u_x\right)^2 + \left(\zeta_y - u_y\right)^2}{\tau} - 1\right]\right), \quad (12)$$

with the reduced local Maxwellians

$$\varphi^M = \frac{n}{\pi\tau}\exp\left[-\frac{\left(\zeta_x - u_x\right)^2 + \left(\zeta_y - u_y\right)^2}{\tau}\right] \text{ and } \psi^M = \frac{n}{2\pi}\exp\left[-\frac{\left(\zeta_x - u_x\right)^2 + \left(\zeta_y - u_y\right)^2}{\tau}\right]. \quad (13)$$

The macroscopic quantities in Eqs. (9)–(13) are readily deduced by applying the same non-dimensionalization and projection procedures to the moments of f and finally they are expressed, in terms of φ and ψ, according to the following double integrals:

$$n\left(x, y\right) = \int_{-\infty}^{\infty}\int_{-\infty}^{\infty} \varphi d\zeta_x d\zeta_y, \quad (14)$$

$$u_x\left(x, y\right) = \frac{1}{n}\int_{-\infty}^{\infty}\int_{-\infty}^{\infty} \zeta_x \varphi d\zeta_x d\zeta_y \quad u_y\left(x, y\right) = \frac{1}{n}\int_{-\infty}^{\infty}\int_{-\infty}^{\infty} \zeta_y \varphi d\zeta_x d\zeta_y, \quad (15)$$

$$\tau\left(x, y\right) = \frac{2}{3n}\int_{-\infty}^{\infty}\int_{-\infty}^{\infty}\left[\left(\zeta_x^2 + \zeta_y^2\right)\varphi + \psi\right] d\zeta_x d\zeta_y - \frac{2}{3}\left(u_x^2 + u_y^2\right), \quad (16)$$

$$p_{xy}\left(x, y\right) = 2\int_{-\infty}^{\infty}\int_{-\infty}^{\infty}\left(\zeta_x - u_x\right)\left(\zeta_y - u_y\right)\varphi d\zeta_x d\zeta_y, \quad (17)$$

$$q_x\left(x, y\right) = \int_{-\infty}^{\infty}\int_{-\infty}^{\infty}\left[\left[\left(\zeta_x - u_x\right)^2 + \left(\zeta_y - u_y\right)^2\right]\varphi + \psi\right]\left(\zeta_x - u_x\right) d\zeta_x d\zeta_y, \quad (18)$$

$$q_y\left(x, y\right) = \int_{-\infty}^{\infty}\int_{-\infty}^{\infty}\left[\left[\left(\zeta_x - u_x\right)^2 + \left(\zeta_y - u_y\right)^2\right]\varphi + \psi\right]\left(\zeta_y - u_y\right) d\zeta_x d\zeta_y. \quad (19)$$

At the boundaries, the reduced distribution functions representing outgoing particles are denoted by φ^+, ψ^+ and they are expressed by the Maxwell purely diffuse reflection as[18]

$$\varphi^+ = \frac{n_w}{\pi\tau_w}\exp\left[-\left(\zeta_x^2 + \zeta_y^2\right)/\tau_w\right] \text{ and } \psi^+ = \frac{n_w}{2\pi}\exp\left[-\left(\zeta_x^2 + \zeta_y^2\right)/\tau_w\right], \quad (20)$$

where τ_w is the dimensionless wall temperature and n_w is a parameter given in terms of the ingoing distributions satisfying the impermeability wall conditions.

Equations (9) and (10), subject to the boundary conditions (20) along with the associated expressions (11-19) provide a complete description of the problem and constitute the basic set of equations to be numerically solved.

B. The numerical scheme

The implemented deterministic algorithm has been repeatedly applied to solve nonlinear flows and heat transfer problems with considerable success.[35–37] A brief description is provided here mainly for completeness purposes.

The problem is solved by discretizing the molecular velocity and physical spaces. In the velocity space it is computationally efficient to present the velocity vector in polar coordinates, according to $\zeta_x = \zeta\cos\theta$ and $\zeta_y = \zeta\sin\theta$. Then, the continuum velocity spectrum (ζ, θ) is replaced by a set of discrete velocities (ζ_m, θ_n), where $\zeta_m \in (0, +\infty)$, $m = 1, 2, \ldots, M$ and $\theta_n \in [0, 2\pi]$, $n = 1, 2, \ldots, N$. The magnitudes ζ_m are taken to be the roots of the Legendre polynomial of order M accordingly mapped from $(-1, 1)$ to $(0, +\infty)$, while the polar angles are $\theta_n = \pi(2n - 1)/N$. The number of discrete velocity vectors is $M \times N$. In the physical space the flow domain is divided into $I \times J$ rectangular elements, with $i = 1, 2, \ldots, I$ and $j = 1, 2, \ldots, J$. The number of points in the physical space is $(I + 1) \times (J + 1)$.

The integro-differential equations (9) and (10) are first discretized in the molecular velocity space and the deduced set of partial differential equations are integrated over each space element defined by the intervals $[x_{i-1/2}, x_{i+1/2}]$ and $[y_{j-1/2}, y_{j+1/2}]$ following a typical second order control volume approach. The moments (14-19) are numerically integrated by applying the trapezoidal rule and Gauss-Legendre quadrature in the polar angle θ and the velocity magnitude ζ, respectively, of the molecular velocity vector. The resulting discretized equations for φ and ψ with the associated discretized moments are solved in an iterative manner which is concluded when the convergence criteria given by

$$\varepsilon^{(k)} = \max_{i,j}\left\{\left|n_{i,j}^{(k)} - n_{i,j}^{(k-1)}\right| + \left|u_{xi,j}^{(k)} - u_{xi,j}^{(k-1)}\right| + \left|u_{yi,j}^{(k)} - u_{yi,j}^{(k-1)}\right| + \left|\tau_{i,j}^{(k)} - \tau_{i,j}^{(k-1)}\right|\right\} \le 10^{-10} \quad (21)$$

is fulfilled. Here, k denotes the iteration index and $\varepsilon^{(k)}$ the error after k iterations. It is noted that upon convergence all conservation principles are accordingly fulfilled. The results presented in Sec. V have been obtained with $M = 80$, $N = 400$, $I = 400$, and $J = 400 \times (H/W)$.

IV. STOCHASTIC MODELING

Stochastic modeling is based on the DSMC method proposed by Bird.[19] In Sec. IV A the specific issues involved in the present implementation of the DSMC method are described. Furthermore, a novel decomposition of the solution into ballistic and collision parts is introduced in the DSMC algorithm, in order to analyze in detail the thermal convection in the enclosure in the transition regime. The methodology to achieve that is described in Sec. IV B, while the results of this decomposition will be provided in Sec. V C.

A. Main characteristics of the implemented DSMC process

The typical DSMC approach is implemented. The gas is represented by a discrete number of model particles, which are evolved in time to statistically mimic the behavior of real molecules. The physical space and time domains are discretized and the real motion of the particles is split into the free motion step, where all particles are traveling a distance proportional to their velocities and the collision step, where particles are interacting, while keeping their positions unchanged. In the first step the particle motion is purely deterministic, while in the second particle collisions are carried out in a stochastic manner.

The collision technique that is employed here is the No Time Counter (NTC) scheme suggested by Bird.[19] A slight modification is introduced in the calculation of the maximum number of collisions N_C in each cell, which is estimated according to[38]

$$N_C = \frac{1}{2}\frac{N\,(N-1)\,F_N\,(\sigma_T c_r)_{\max}\,\Delta t}{V_C}, \quad (22)$$

where N is the actual number of particles in cell, F_N is the number of real particles represented by a simulator, $(\sigma_T c_r)_{\max}$ is the maximum value of the product of the collision cross section and the

relative velocity of the particles in the collision (this quantity is updated throughout the simulation), Δt is the time step, and V_C is the volume of the cell.

In addition to the NTC scheme, an alternative model, which allows the use of a small average number of particles in each cell and avoids repeated collisions, the so called Simplified Bernoulli Trails (SBT) scheme,[39] has been also applied. The results obtained by both collision schemes are in excellent agreement, even when the average number of particles in cells in the SBT scheme has been reduced to unity.

The space domain has been discretized by using squared cells ($\Delta x = \Delta y$), with $\Delta x = 0.01$, i.e., 100 cells have been taken in the x-direction, while the number of cells in the y-direction depends on the aspect ratio H/W and it is equal to $n_C = 100 \times (H/W)$. The number of particles per cell on the NTC scheme is fixed to 25 and the time step is chosen to be sufficiently smaller (about 1/3) than the cell traversal time, defined as $W/(n_C \upsilon_0)$. The macroscopic quantities, defined by Eq. (2), are volume based calculated by averaging the microscopic values of the particles at a given cell and are given by the following summations:

$$n = \frac{\sum_{k=1}^{S} N(t_k)}{SV_C} = \frac{N_T}{SV_C}, \tag{23}$$

$$u_x = \frac{1}{N_T}\sum_{k=1}^{S}\sum_{i=1}^{N(t_k)} \zeta_{x,i}(t_k) \qquad u_y = \frac{1}{N_T}\sum_{k=1}^{S}\sum_{i=1}^{N(t_k)} \zeta_{y,i}(t_k), \tag{24}$$

$$\tau_\alpha = \frac{1}{N_T}\sum_{k=1}^{S}\sum_{i=1}^{N(t_k)} \left(\zeta_{\alpha,i}\right)^2 - \left(\frac{1}{N_T}\sum_{k=1}^{S}\sum_{i=1}^{N(t_k)} \zeta_{\alpha,i}\right)^2, \quad \alpha = \{x, y, z\}, \quad \tau = 2\left(\tau_x + \tau_y + \tau_z\right)/3, \tag{25}$$

$$p_{xy} = \frac{1}{N_T}\sum_{k=1}^{S}\sum_{i=1}^{N(t_k)} \left(\zeta_{x,i}\zeta_{y,i}\right) - u_x u_y, \tag{26}$$

$$\begin{aligned} q_x = {} & \frac{1}{N_T}\sum_{k=1}^{S}\sum_{i=1}^{N(t_k)} \zeta_{x,i}\left(\zeta_{x,i}^2 + \zeta_{y,i}^2 + \zeta_{z,i}^2\right) - 2u_x \frac{1}{N_T}\sum_{k=1}^{S}\sum_{i=1}^{N(t_k)} \left(\zeta_{x,i}^2 - u_x^2\right) \\ & -2u_y \frac{1}{N_T}\sum_{k=1}^{S}\sum_{i=1}^{N(t_k)} \left(\zeta_{x,i}\zeta_{y,i} - u_x u_y\right) - u_x \frac{1}{N_T}\sum_{k=1}^{S}\sum_{i=1}^{N(t_k)} \left(\zeta_{x,i}^2 + \zeta_{y,i}^2 + \zeta_{z,i}^2\right), \end{aligned} \tag{27}$$

$$\begin{aligned} q_y = {} & \frac{1}{N_T}\sum_{k=1}^{S}\sum_{i=1}^{N(t_k)} \zeta_{y,i}\left(\zeta_{x,i}^2 + \zeta_{y,i}^2 + \zeta_{z,i}^2\right) - 2u_x \frac{1}{N_T}\sum_{k=1}^{S}\sum_{i=1}^{N(t_k)} \left(\zeta_{x,i}\zeta_{y,i} - u_x u_y\right) \\ & -2u_y \frac{1}{N_T}\sum_{k=1}^{S}\sum_{i=1}^{N(t_k)} \left(\zeta_{y,i}^2 - u_y^2\right) - u_y \frac{1}{N_T}\sum_{k=1}^{S}\sum_{i=1}^{N(t_k)} \left(\zeta_{x,i}^2 + \zeta_{y,i}^2 + \zeta_{z,i}^2\right). \end{aligned} \tag{28}$$

In Eqs. (23)–(28), N_T is the total number of sampled particles, S denotes the number of samples, t_k indicates the different times over which the sampling is performed, and $N(t_k)$ is the number of particles in the cell at time t_k. It is noted that the macroscopic properties are obtained by time averaging over $S = 5 \times 10^5$ time steps after the steady-state regime has been recovered.

B. Decomposition of the solution into ballistic and collision parts

In general, a kinetic solution at some point in a flow domain consists of two parts, namely, the ballistic and the collision parts. The former one is due to particles arriving at this point from the

boundaries with no collisions, while the latter one is due to particles arriving at this point after an arbitrary number of collisions (at least one).

The ballistic and collision parts of the solution of the thermally induced flow in the enclosure are computed separately and the contribution of each part to the overall solution is analyzed. The dimensionless distribution function $g = g(x, y, \boldsymbol{\zeta})$ at a local point (x, y), defined in Sec. III A, is decomposed as

$$g(x, y, \boldsymbol{\zeta}) = g^{(b)}(x, y, \boldsymbol{\zeta}) + g^{(c)}(x, y, \boldsymbol{\zeta}), \tag{29}$$

where $g^{(b)}$ and $g^{(c)}$ denote the ballistic and collision parts of the distribution function, respectively. It is noted that particles contributing to the ballistic part of the solution at point (x, y) may collide to other particles in their movement after that point. Therefore, the two parts of the solution are named ballistic and collision in order to distinguish this splitting from the typical free molecular and collisional decomposition, as well as from other decompositions of the distribution function, which have been previously introduced to treat boundary induced discontinuities.[40–42]

The prescribed decomposition of the particle distribution in a given cell of the computational grid with center point (x, y) can be implemented in the basic DSMC algorithm by making some additions in the indexing stage. More specifically, all model particles $j = 1, \ldots, N_T$ taking place in the simulation are tagged by introducing the indicator I_j, which has the value of 0 or 1 indicating if a particle contributes to the ballistic or the collision part of the distribution, respectively. A particle passes into the ballistic part when it is reflected from a wall and goes into the collision part when interacts with another particle. The indicator is set to 0 each time that a particle is reflected from the bounding walls of the enclosure, while in the stage of particle free motion the indicators are not changed. In the stage of binary collisions the indicators (I_j, I_k) of any pair of particles (j, k) involved in a collision are set to 1. During the simulation process the particle indicators may change their values all the time. In the sampling stage of the macroscopic properties at given time t_m all particles with indicators $I_j = 0$, are considered belonging to the ballistic part of the particle distribution and all particles with indicators $I_j = 1$ to the collision part. As a result, the total number of all particles accumulated in a cell is divided into two groups $N_T = N_b + N_c$ and the macroscopic quantities defined by Eqs. (23)–(28) are sampled into the two corresponding parts.

In the present work we are mainly interested to the distributions of number density and velocity components which are decomposed according to

$$n(x, y) = n^{(b)}(x, y) + n^{(c)}(x, y), \tag{30}$$

$$u_x(x, y) = u_x^{(b)}(x, y) + u_x^{(c)}(x, y), \tag{31}$$

$$u_y(x, y) = u_y^{(b)}(x, y) + u_y^{(c)}(x, y), \tag{32}$$

where the superscripts (b) and (c) denote the ballistic and collision parts of the distributions, respectively. They are computed as follows: Taking into consideration, e.g., for u_x, that

$$u_x(x, y) = \frac{1}{n}\int \zeta_x g d\zeta = \frac{1}{n}\int \zeta_x g^{(b)} d\zeta + \frac{1}{n}\int \zeta_x g^{(c)} d\zeta = u_x^{(b)}(x, y) + u_x^{(c)}(x, y) \tag{33}$$

the ballistic and collision parts are computed through the DSMC code by the summations

$$u_x^{(b)} = \frac{1}{N_T}\sum_{k=1}^{S}\sum_{i=1}^{N(t_k)}[1 - I_i(t_k)]\,\zeta_{x,i}(t_k) \quad \text{and} \quad u_x^{(c)} = \frac{1}{N_T}\sum_{k=1}^{S}\sum_{i=1}^{N(t_k)} I_i(t_k)\,\zeta_{x,i}(t_k), \tag{34}$$

respectively, while the velocities $\zeta_{x,i}^{(b)}$ and $\zeta_{x,i}^{(c)}$ are related to the corresponding particles. The decomposition of the number density and the y-component of the velocity and their computation is performed in an analogous manner.

Based on the above description it is deduced that for the ballistic part of the particle distribution the boundaries act as a source, while the bulk flow acts as a sink. The situation is reversed for the collision part of the particle distribution, where the bulk flow acts as a distributed source and the

walls as a sink. Computational results of this decomposition are presented in Sec. V C providing an insight view and a better understanding of the overall solution of the problem.

V. RESULTS AND DISCUSSION

Results are provided for all macroscopic quantities of theoretical importance and practical interest in a wide range of the Knudsen number ($0.01 \leq Kn_0 \leq 10$) covering the whole transition regime as well as parts of the slip and free molecular regimes and for temperature ratios $T_C/T_H = 0.1$, 0.5, and 0.9 corresponding to large, moderate, and small temperatures differences between the top and bottom plates, respectively. Enclosures with aspect ratios $H/W = 0.5, 1, 2$ are considered. Most of the results are for hard sphere molecules ($\omega = 1/2$), while some results for Maxwell molecules ($\omega = 1$) are provided as well.

In the case of the large temperature difference $T_C/T_H = 0.1$, simulations have been performed for all Knudsen numbers and aspect ratios by both the deterministic solver of the Shakhov model equation and the DSMC solver. The agreement between the corresponding results produced by these two completely different approaches is always very good as it is indicatively demonstrated for some cases in Subsections V A and V B. In the cases of $T_C/T_H = 0.5$ and 0.9 simulations have been performed mainly by the deterministic solver.

The macroscopic description of the whole flow domain of the enclosure in terms of the flow parameters is given in Sec. V A and then, in Sec. V B the discussion is focused on the behavior of the macroscopic quantities along the enclosure walls. Finally, in Sec. V C, the solution is split into the ballistic and collision parts, based on the methodology previously presented in Sec. IV B, and the flow behavior along the lateral walls is explained. All results are in dimensionless form.

A. Flow domain

The effect of the degree of the gas rarefaction on the patterns of the flow field is shown in Fig. 2, where the velocity streamlines superimposed on the temperature contours for $Kn_0 = 0.01$, 0.1, 0.2, 0.5, 1, and 10 in a square enclosure with $T_C/T_H = 0.1$ are presented. The flow is symmetric about $x = 0$. It is seen that for $Kn_0 = 0.01$ only the two Vortex-type I are observed and the gas flows next to the lateral walls from the colder towards the hotter region (from top to bottom). At $Kn_0 = 0.1$, at the two bottom corners of the enclosure, Vortex-type II start to appear counter rotating to the other ones. As the Knudsen number is increased, they are gradually increased as well, and for $Kn_0 = 0.5$, 1, and 10 these eddies of type II are well developed and cover large portions of the flow domain with the gas flowing along the whole length of the side walls from the hotter to the colder region (from bottom to top). The two Vortex-type I have been squeezed towards the top and the center of the cavity. The temperature contours indicate that the flow domain is thermally stratified and as expected, the temperature jump at the walls becomes larger as the Knudsen number is increased. In general, as the flow becomes more rarefied the hot-to-cold motion next to the lateral walls is enhanced and the structure of the flow pattern becomes more complex. Of course as the Knudsen number tends to infinity the gas velocity vanishes.

It may be interesting to note that while in the classical lid driven cavity problem as we are approaching the hydrodynamic regime (i.e., as the Knudsen number is decreased) the flow becomes more complex with secondary vortices added to the main ones, here on the contrary the interesting flow patterns with the Vortex-type II eddies, start to appear as we are moving into the transition regime (i.e., as the Knudsen number is increased). Overall, the degree of gas rarefaction significantly influences the thermally driven flow in the enclosure.

Figure 3 shows also streamlines and temperature contours in a square cavity for the cases of moderate and small temperature differences, namely, $T_C/T_H = 0.5$ and 0.9, respectively, and for the typical values of $Kn_0 = 0.1$, 1, and 10. These results along with the corresponding ones in Fig. 2 are helpful to describe the effect of the temperature ratio on the flow pattern. In general, for the same Kn_0, as the temperature difference between the bottom and top plates, as well as the temperature gradient along the lateral walls, are decreased, the Vortex-type II with the hot-to-cold flow in the vicinity of the walls become thinner covering a smaller portion of the flow domain. For the small

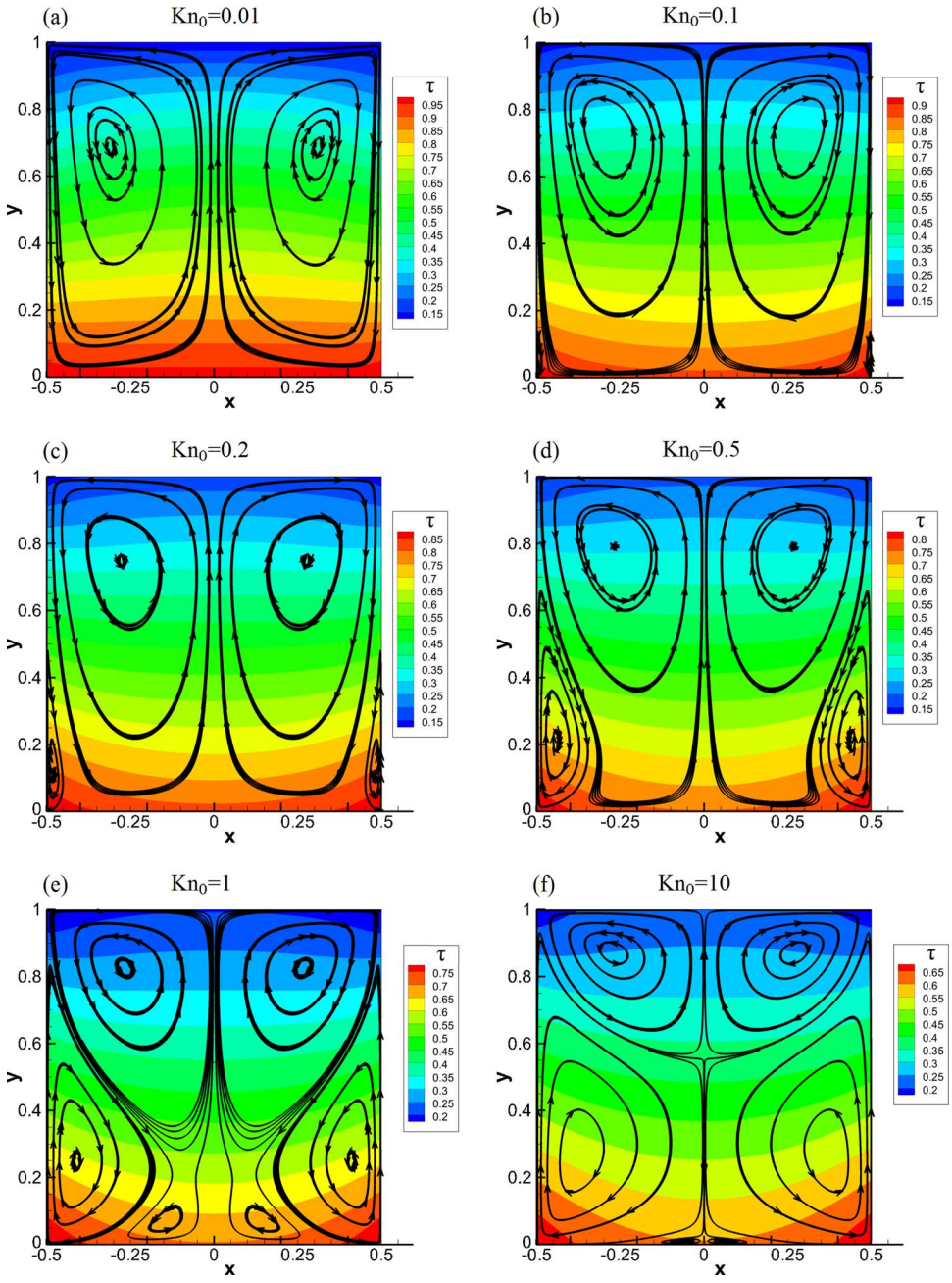

FIG. 2. Streamlines and temperature contours in a square enclosure for $T_C/T_H = 0.1$ and various Knudsen numbers.

temperature difference of $T_C/T_H = 0.9$ at $Kn_0 = 1$ these eddies are very thin but still cover the whole length of the non-isothermal side walls and then as the temperature difference is increased they are grown pushing the Vortex-type I towards the center.

A more quantitative description of the flow is provided in Fig. 4, where the x and y components of the macroscopic velocity on vertical and horizontal planes, respectively, passing through the centers of the Vortex-type I are plotted. The results are for a square enclosure with $T_C/T_H = 0.1$ with $Kn_0 = 0.01$, 0.1, and 1. The u_y profiles are plotted versus $x \in [-0.5, 0.5]$ and the u_x profiles are plotted versus $y \in [0, 1]$. Both deterministic and stochastic results are shown and it is seen that the agreement is always very good. The distributions of u_y are symmetric about $x = 0$ and the points where u_y changes sign correspond to the x coordinate of the center of the two eddies of type I. The

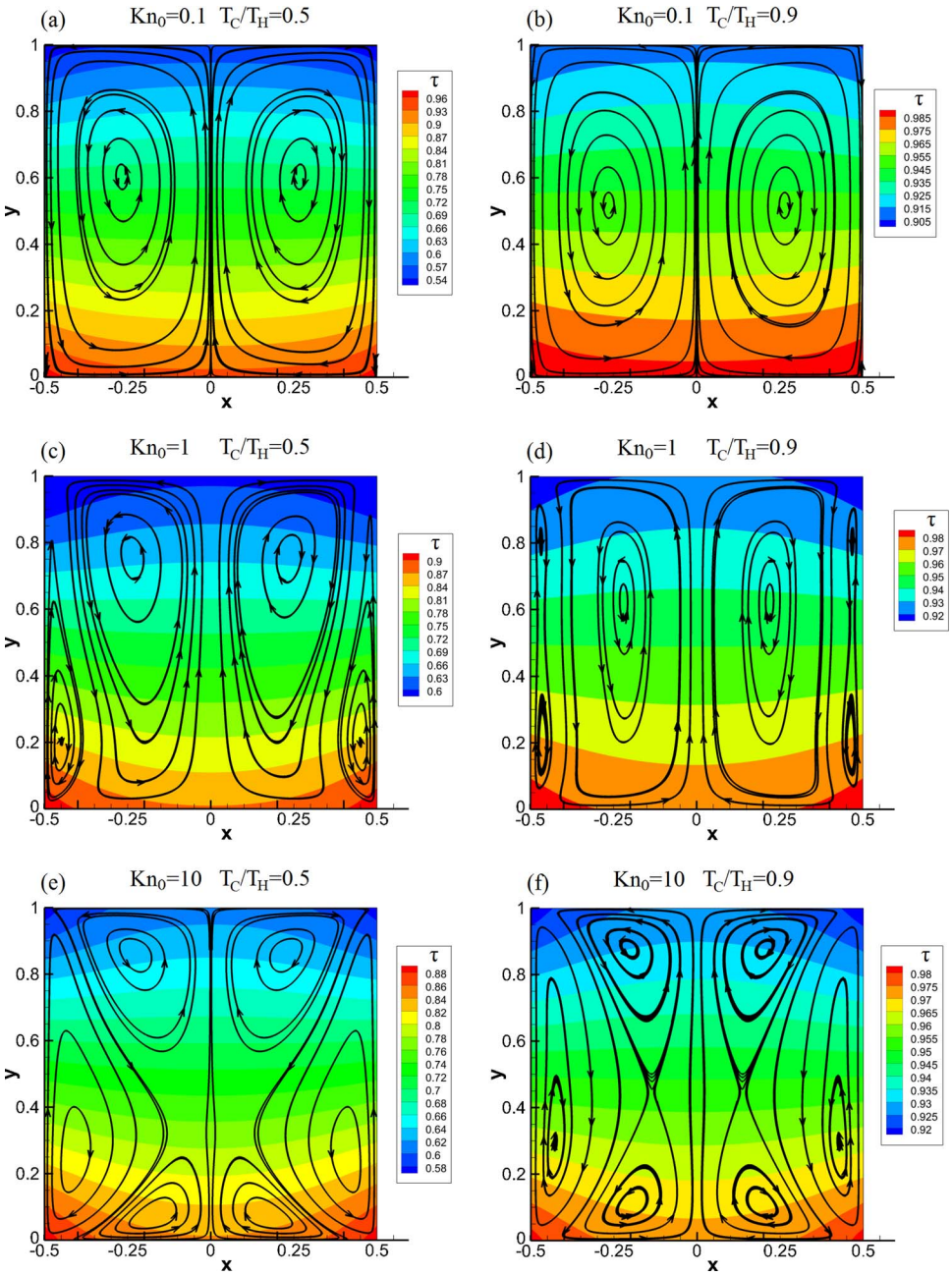

FIG. 3. Streamlines and temperature contours in a square enclosure for various Knudsen numbers and temperature ratios.

distributions of u_x are changing sign in the case of $Kn_0 = 0.01$ and 0.1 only once, which implies that only the two Vortex-type I are present (actually for $Kn_0 = 0.1$ the Vortex-type II has been created but it is not extended up to horizontal axis passing through the centers of the Vortex-type I). In the case of $Kn_0 = 1$ the distributions of u_x are changing sign several times, which indicates that both Vortex-type I and II are present. These observations are in accordance to the flow patterns shown in Fig. 2 for the corresponding Knudsen numbers. In all cases the maximum absolute value of the velocities is small, approximately in the order of 10^{-2} or even less (the local Mach is about 10% higher than the reported velocity magnitudes), which is typical in rarefied thermally driven flows. Comparing between the absolute values of the velocity for various Knudsen numbers it is seen that the maximum values are at $Kn_0 = 0.1$. Also, as the Knudsen number is increased the magnitude of

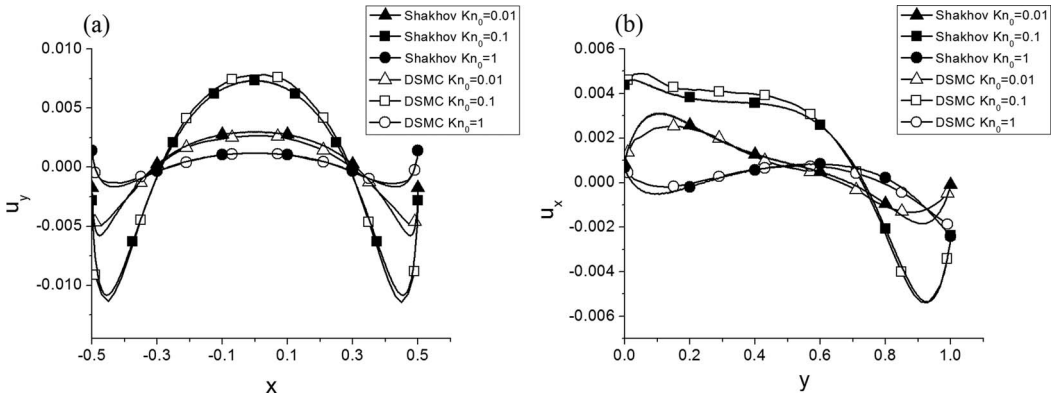

FIG. 4. Distributions of the (a) y and (b) x components of the velocity on vertical and horizontal planes, respectively, passing through the centers of the two Vortex-type I for a square enclosure with $T_C/T_H = 0.1$ and various Knudsen numbers.

the velocities u_y related to Vortex-type II, in Fig. 4(b), is increased and may become even larger than that of Vortex-type I.

These latter remarks are confirmed by the dimensionless flow rates of the Vortex- type I and II presented in Tables I and II respectively, for various temperature ratios and reference Knudsen numbers. The former ones are computed by integrating the dimensionless flux nu_x in the y direction from the center of the Vortex-type I to the top wall and the latter ones by integrating the flux nu_y in the x direction from the center of Vortex-type II to the side wall. The tabulated results have been obtained by the deterministic solution of the Shakhov model equation. Also, flow rates have been obtained by the DSMC approach for the case of $T_C/T_H = 0.1$ and they are in very good agreement with the corresponding tabulated ones. It is seen in Table I that starting from $Kn_0 = 0.01$ as the Knudsen number is increased and for the same temperature ratio, the flow rate of Vortex-type I is increased obtaining a maximum value around $Kn_0 = 0.07$ and then is constantly decreased as the Knudsen number keeps increasing. This is valid for all three temperature ratios. The corresponding flow rates of Vortex-type II in Table II, indicate a maximum flow rate around $Kn_0 = 1.2$. The exact physical reasoning for these maximum flow rates with regard to the reference Knudsen number is contributed to the number of collisions between particles and between particles and boundaries as the gas rarefaction is changing. In addition, while for $Kn_0 \leq 0.1$ the flow rate of Vortex-type II is several orders of magnitudes smaller compared to the corresponding ones of Vortex-type I, as the Knudsen number is increased the two flow rates become of the same order and in some cases the former ones are even larger. Also, for the same Knudsen number as the temperature difference is increased the flow rate, as expected, is also increased.

The effect of the lateral walls on the flow pattern may be seen in Fig. 5, where the streamlines and temperature contours for two rectangular enclosures, namely, $H/W = 0.5$ and 2 for the specific case of $T_C/T_H = 0.1$ and $Kn_0 = 1$ are plotted. Observing these flow fields along with the corresponding one for a square cavity ($H/W = 1$) in Fig. 2, it is seen that as the aspect ratio is increased the presence of the Vortex-type II becomes more dominant covering a larger part of the flow domain. Obviously, as the aspect ratio is increased, i.e., as the depth prevails over the width of the cavity, the importance of the non-isothermal side walls compared to the bottom and top walls is also increased.

TABLE I. Dimensionless flow rate of Vortex-type I in a square enclosure for various Kn_0 and T_C/T_H.

	Kn_0						
T_C/T_H	0.01	0.06	0.07	0.08	0.1	1	10
0.1	6.34(−4)	1.70(−3)	1.72(−3)	1.71(−3)	1.67(−3)	2.89(−4)	2.76(−5)
0.5	2.87(−4)	7.51(−4)	7.53(−4)	7.44(−4)	7.08(−4)	8.60(−5)	6.38(−6)
0.9	5.07(−5)	1.31(−4)	1.31(−4)	1.30(−4)	1.23(−4)	1.21(−5)	6.99(−7)

TABLE II. Dimensionless flow rate of Vortex-type II in a square enclosure for various Kn_0 and T_C/T_H.

	Kn_0						
T_C/T_H	0.01	0.06	0.07	0.08	0.1	1	10
0.1	2.55(−6)	1.18(−4)	1.198(−4)	1.204(−4)	1.202(−4)	3.99(−5)	2.55(−6)
0.5	6.98(−7)	2.46(−5)	2.504(−5)	2.513(−5)	2.512(−5)	8.70(−6)	6.98(−7)
0.9	8.41(−8)	2.85(−6)	2.902(−6)	2.936(−6)	2.942(−6)	1.08(−6)	8.41(−8)

The computed dimensionless flow rates of the Vortex type I and II are also changing significantly with the aspect ratio. It is concluded that the aspect ratio is a very important factor in this flow configuration.

Since this is a thermally induced flow it is reasonable to investigate the effect of the intermolecular collision model and this is done by including in Fig. 6, some results for Maxwell molecules for the specific cases of $T_C/T_H = 0.1$, with $Kn_0 = 0.1$ and 1. Comparing the plotted streamlines and temperature contours with the corresponding ones for hard spheres in Fig. 2, it is observed that for $Kn_0 = 0.1$ there is actually no effect, while for $Kn_0 = 1$ there are differences. This remark is also confirmed by the computed dimensionless flow rates of Vortex type I and II. It may be stated that as the intermolecular interaction becomes softer the region occupied by the Vortex-type II is reduced and the cold-to-hot flow becomes less intensive. However, again the hot-to-cold motion appears as the Knudsen number is increased.

B. Non-isothermal cavity walls

Here, a more thorough description of the macroscopic quantities in the vicinity of the boundaries of the enclosure is provided. This includes the y components of the velocity and heat flux as well as the shear stress along the lateral walls and the average heat flux from the bottom wall. Some comments on the range of validity of the mechanism explaining the formation of Vortex-type II, as described in Ref. 14, are included.

In Table III, the tangential velocity u_y along the lateral walls of a square enclosure for small, moderate, and large temperature differences in a wide range of the reference Knudsen number are provided. Due to symmetry these results correspond to $x = \mp 1/2$. When $u_y < 0$, the flow is from the top to bottom and corresponds to the expected thermal type flow as described by the Vortex-type

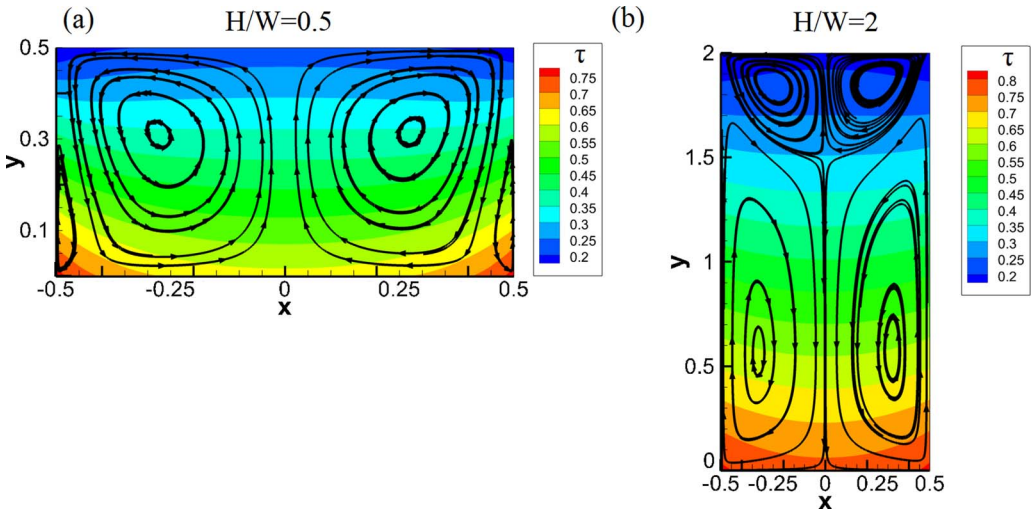

FIG. 5. Streamlines and temperature contours in rectangular enclosures of (a) $H/W = 0.5$ and (b) $H/W = 2$, for $T_C/T_H = 0.1$ and $Kn_0 = 1$.

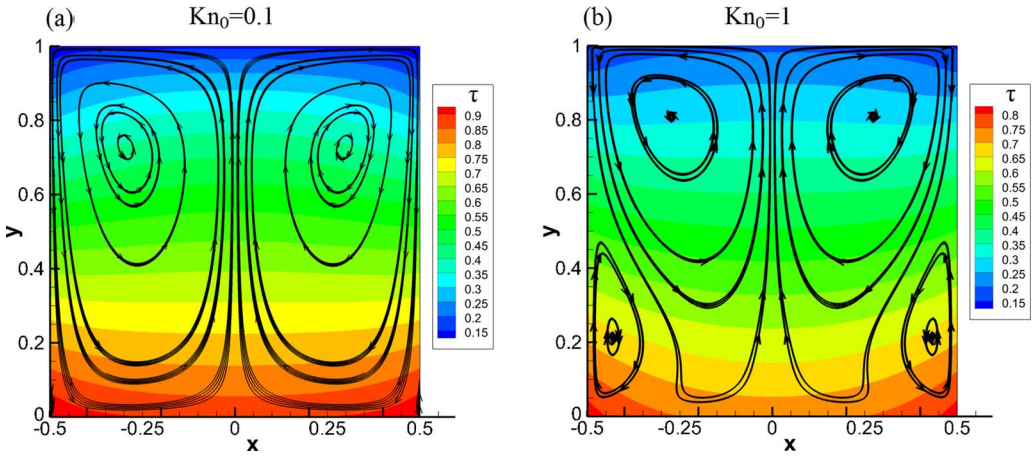

FIG. 6. Streamlines and temperature contours in a square enclosure with (a) $Kn_0 = 0.1$ and (b) $Kn_0 = 1$ for Maxwell molecules ($\omega = 1$).

I pattern, while when $u_y > 0$ the flow is the other way around and corresponds to the unexpected flow pattern as described by Vortex-type II. It is observed that when $Kn_0 = 0.01$ the values of u_y are negative and only very close to $y = 0$ and 1 very small positive values may appear. The Vortex-type I flow covers the whole flow domain. When $Kn_0 = 1$ and 10 the values of u_y are always positive, which implies that the Vortex-type II flow covers the whole length of the lateral walls. Finally, for $Kn_0 = 0.1$ both positive and negative values of u_y are observed. The positive values are close to the two ends and the negative values in the middle part of the wall. That implies that although the Vortex-type I flow still covers most of the whole flow field, counter rotating vortices at the bottom and top corners have been created, which, as the Knudsen number is increased, they grow and merge into a Vortex-type II along the whole length of the side wall. These observations qualitatively hold for all three temperature ratios. Combining these results with the previous ones in Sec. V A it is concluded that in small Knudsen numbers the expected thermal creep flow prevails and then for $Kn_0 \geq 0.5$ the importance of the unexpected hot-to-cold flow is gradually increased and its presence significantly effects both qualitatively and quantitatively the flow configuration.

According to the R13 approach in Ref. 14, the formation of the Vortex-type II is explained by the opposite contribution of the two different terms of the tangential velocity at the wall, which in

TABLE III. Tangential velocity u_y along the lateral walls of a square enclosure for various Knudsen numbers and temperature ratios.

$\frac{T_C}{T_H}$	Kn_0	y 0.05	0.15	0.25	0.35	0.45	0.55	0.65	0.75	0.85	0.95
0.1	0.01	−5.1(−4)	−1.5(−3)	−1.9(−3)	−2.0(−3)	−2.0(−3)	−1.9(−3)	−1.8(−3)	−1.6(−3)	−1.3(−3)	−8.4(−4)
	0.1	1.7(−3)	8.8(−4)	−1.5(−4)	−1.1(−3)	−1.8(−3)	−2.5(−3)	−2.8(−3)	−2.8(−3)	−2.0(−3)	−5.9(−5)
	1	5.4(−3)	5.8(−3)	5.6(−3)	5.0(−3)	4.4(−3)	3.6(−3)	2.8(−3)	1.9(−3)	1.2(−3)	7.7(−4)
	10	1.3(−3)	1.3(−3)	1.2(−3)	1.1(−3)	9.2(−4)	7.4(−4)	5.7(−4)	3.9(−4)	2.5(−4)	1.3(−4)
0.5	0.01	−2.8(−4)	−6.5(−4)	−7.7(−4)	−8.0(−4)	−8.1(−4)	−7.9(−4)	−7.6(−4)	−7.1(−4)	−6.1(−4)	−3.5(−4)
	0.1	5.6(−4)	−2.2(−5)	−5.2(−4)	−8.6(−4)	−1.1(−3)	−1.2(−3)	−1.1(−3)	−9.1(−4)	−4.4(−4)	3.2(−4)
	1	1.5(−3)	1.6(−3)	1.5(−3)	1.4(−3)	1.2(−3)	1.1(−3)	1.0(−3)	9.4(−4)	9.2(−4)	8.7(−4)
	10	3.4(−4)	3.5(−4)	3.2(−4)	2.9(−4)	2.6(−4)	2.3(−4)	2.2(−4)	2.0(−4)	1.9(−4)	1.8(−4)
0.9	0.01	−5.5(−5)	−1.1(−4)	−1.3(−4)	−1.4(−4)	−1.4(−4)	−1.4(−4)	−1.4(−4)	−1.3(−4)	−1.1(−4)	−5.7(−5)
	0.1	8.2(−5)	−3.5(−5)	−1.2(−4)	−1.7(−4)	−2.0(−4)	−2.0(−4)	−1.8(−4)	−1.3(−4)	−4.6(−5)	7.6(−5)
	1	2.2(−4)	2.3(−4)	2.1(−4)	2.0(−4)	1.9(−4)	1.9(−4)	1.9(−4)	2.0(−4)	2.1(−4)	2.0(−4)
	10	4.6(−5)	4.8(−5)	4.6(−5)	4.3(−5)	4.2(−5)	4.1(−5)	4.1(−5)	4.3(−5)	4.4(−5)	4.2(−5)

TABLE IV. Shear stress p_{xy} along the lateral wall at $x = -0.5$ of a square enclosure for various Knudsen numbers and temperature ratios.

		y					
T_C/T_H	Kn_0	0	0.2	0.4	0.6	0.8	1.0
0.1	0.01	1.4(−3)	7.7(−4)	5.1(−4)	4.1(−4)	4.3(−4)	2.1(−3)
	0.1	1.0(−2)	1.2(−2)	1.3(−2)	1.3(−2)	1.5(−2)	2.1(−2)
	1	3.1(−2)	3.8(−2)	4.3(−2)	4.5(−2)	4.6(−2)	4.5(−2)
	10	4.3(−2)	4.9(−2)	5.3(−2)	5.5(−2)	5.4(−2)	5.0(−2)
0.5	0.01	9.1(−4)	3.5(−4)	2.4(−4)	2.2(−4)	2.8(−4)	1.0(−3)
	0.1	7.0(−3)	7.5(−3)	7.5(−3)	7.6(−3)	8.1(−3)	8.7(−3)
	1	2.2(−2)	2.6(−2)	2.8(−2)	2.8(−2)	2.8(−2)	2.5(−2)
	10	2.9(−2)	3.3(−2)	3.5(−2)	3.5(−2)	3.4(−2)	3.1(−2)
0.9	0.01	1.9(−4)	6.4(−5)	4.5(−5)	4.4(−5)	6.2(−5)	2.0(−4)
	0.1	1.5(−3)	1.6(−3)	1.5(−3)	1.5(−3)	1.6(−3)	1.6(−3)
	1	4.7(−3)	5.4(−3)	5.7(−3)	5.7(−3)	5.4(−3)	4.8(−3)
	10	6.0(−3)	6.7(−3)	7.1(−3)	7.1(−3)	6.8(−3)	6.1(−3)

the present notation, is written as

$$u_y^{R13} = -\frac{1}{(\tau n + 0.5 p_{yy})}\left(\frac{\sqrt{\pi\tau}}{2} p_{xy} + \frac{1}{5} q_y\right). \tag{35}$$

The superscript R13 has been added here, in order to distinguish in our discussion the tangential velocity obtained by Eq. (35) from the one (u_y) obtained by the kinetic solution. The first term in the parenthesis corresponds to the viscous part of the tangential wall velocity and the second one to the transpirational part, caused by the shear stress and the tangential heat flux, respectively. The respective magnitude of these terms determines the sign of the tangential velocity and the local direction of the flow along the side walls. In order to examine the validity of this theory, the kinetic results of p_{xy} and q_y are introduced to compute, according to Eq. (35), the viscous and transpirational parts of the wall tangential velocity and the whole velocity as well.

The shear stress p_{xy} and the tangential heat flux q_y along the lateral wall at $x = -1/2$ of a square enclosure for various Knudsen numbers and temperature ratios are provided in Tables IV and V, respectively. It is seen that always $p_{xy} < 0$ and $q_y > 0$, i.e., they indeed have an opposite contribution to the tangential velocity. Since, however, as the Knudsen number is increased, both the values of the heat flux and the absolute values of the shear stresses are increased, it is necessary to further compute the contribution of each part separately.

In Fig. 7, the tangential velocities obtained by kinetic theory and according to Eq. (35), denoted by u_y and u_y^{R13}, respectively, for $Kn_0 = 0.01$, 0.05, 0.1, and 1, are plotted. When the velocity distributions are negative the transpirational part of the solution dominates and the flow along the lateral walls is from cold-to-hot (Vortex-type I), while when they are positive the viscous part dominates and the flow is from hot-to-cold (Vortex-type II). The agreement between the kinetic and R13 theory in small Knudsen numbers is very good and then, as the flow becomes more rarefied, the discrepancies, as expected, are increased. In general, the good qualitative agreement for $Kn_0 \leq 0.1$ indicates that the theory developed in Ref. 14 in order to explain the formation of the hot-to-cold flow in the vicinity of the walls is valid in the slip regime and fails as the Knudsen number is increased. In Sec. V C a reasonable explanation for this type of flow in the whole range of the Knudsen number is provided.

It has been pointed in Sec. V A that the aspect ratio of the enclosure effects significantly the flow configuration and quantities. To further demonstrate the effect of the lateral walls, the tangential velocity and heat flux along the lateral walls of enclosures with $H/W = 0.5$, 1, and 2 for $T_C/T_H = 0.1$ and $Kn_0 = 1$ are plotted in Fig. 8. For the specific Knudsen number and temperature ratio the velocities are positive for all three aspect ratios and approximately of the same magnitude resulting

TABLE V. Tangential heat flux q_y along the lateral wall at $x = -0.5$ of a square enclosure for various Knudsen numbers and temperature ratios.

		y					
T_C/T_H	Kn_0	0	0.2	0.4	0.6	0.8	1.0
0.1	0.01	5.5(−3)	7.2(−3)	6.7(−3)	5.8(−3)	4.6(−3)	2.1(−3)
	0.1	3.5(−2)	4.1(−2)	4.5(−2)	4.5(−2)	4.2(−2)	3.3(−2)
	1	8.9(−2)	9.9(−2)	1.1(−1)	1.1(−1)	1.1(−1)	1.0(−1)
	10	1.2(−1)	1.3(−1)	1.3(−1)	1.3(−1)	1.3(−1)	1.2(−1)
0.5	0.01	3.2(−3)	4.4(−3)	4.2(−3)	3.9(−3)	3.7(−3)	2.4(−3)
	0.1	2.5(−2)	3.0(−2)	3.2(−2)	3.2(−2)	3.0(−2)	2.4(−2)
	1	7.7(−2)	8.3(−2)	8.7(−2)	8.8(−2)	8.6(−2)	8.0(−2)
	10	1.0(−1)	1.1(−1)	1.1(−1)	1.1(−1)	1.1(−1)	1.0(−1)
0.9	0.01	6.5(−4)	9.2(−4)	9.1(−4)	9.1(−4)	8.9(−4)	6.2(−4)
	0.1	5.7(−3)	6.9(−3)	7.3(−3)	7.3(−3)	6.9(−3)	5.6(−3)
	1	1.8(−2)	2.0(−2)	2.0(−2)	2.0(−2)	2.0(−2)	1.8(−2)
	10	2.3(−2)	2.5(−2)	2.6(−2)	2.6(−2)	2.5(−2)	2.3(−2)

to stiffer velocity gradients as H/W is decreased. The tangential heat flux is significantly increased as H/W is decreased, i.e., as the effect of the side walls is decreased.

Closing this subsection the average dimensionless heat flux directed from the bottom plate into the enclosure is estimated by integrating the heat flux $q_y(x, 0)$ over the distance $x \in$ b$[-0.5, 0.5]$. In Table VI, the average dimensionless heat flux, denoted by q_{av} is given in terms of the reference Knudsen number Kn_0 for $T_C/T_H = 0.1, 0.5$, and 0.9. The corresponding results obtained by the DSMC method, using 400 cells in each direction and 100 particles per cell, are also included for comparison purposes. The agreement between the corresponding Shakhov and the DSMC results is excellent. As it is seen when the temperature difference between the top and bottom plates is increased the average heat flux for the same Kn_0, as expected, is also increased. Although not shown in the table it is noted that as H/W is increased the average heat flux is decreased, e.g., the computed values of q_{av} in the case of $T_C/T_H = 0.1$ for $H/W = 0.5$, 1, and 2 are 0.35, 0.14, and 0.057, respectively. Concerning the effect of the collision parameter ω on q_{av} it turns out that it is small since the values of the computed average heat fluxes for hard sphere and Maxwell molecules are close.

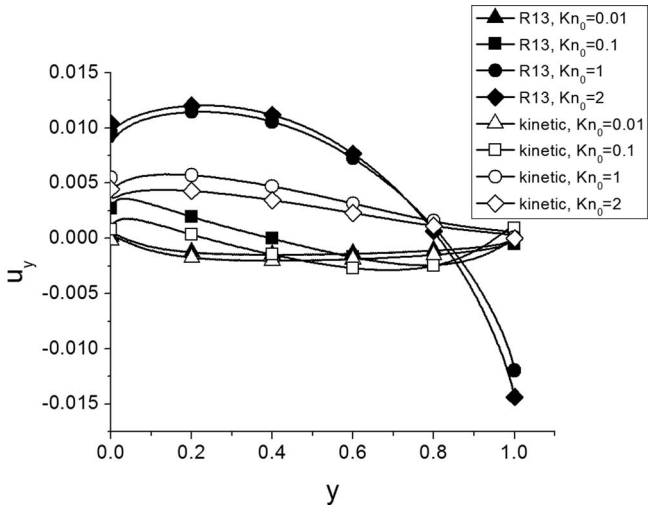

FIG. 7. Tangential velocity u_y along the lateral walls of a square enclosure for $T_C/T_H = 0.1$ and various Kn_0 computed by the present kinetic approach and by Eq. (35) based on the R13 approach.

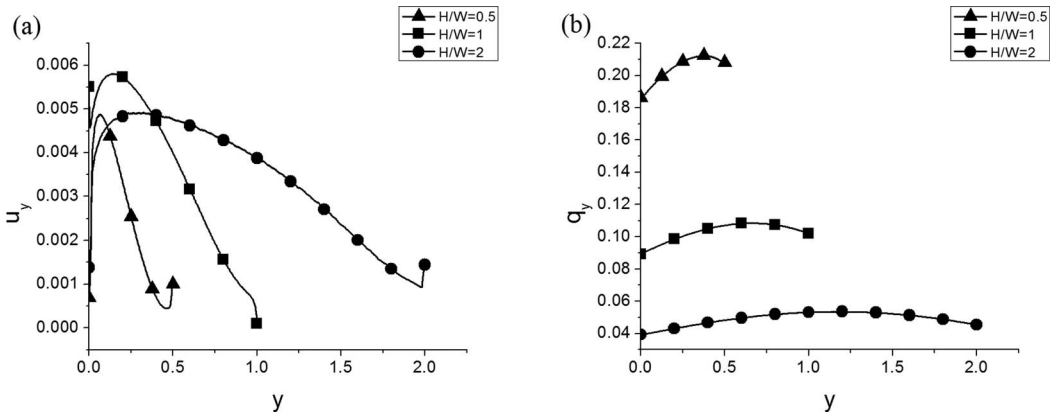

FIG. 8. Distributions of the tangential (a) velocity u_y and (b) heat flux q_y along the lateral walls of rectangular enclosures with various aspect ratios for $T_C/T_H = 0.1$ and $Kn_0 = 1$.

C. Ballistic and collision contributions

The decomposition of the DSMC solution into the ballistic and collision parts, as described in Sec. IV B, is applied in a square enclosure for $Kn_0 = 0.05$ and 2, with $T_C/T_H = 0.1$. The two values of the reference Knudsen numbers have been chosen as representatives to demonstrate the contribution of the ballistic and collision parts to the overall solution in the slip and transition regimes. In addition, the corresponding results are typical for analyzing the thermal effects on the flow configuration in small and large Knudsen numbers.

The streamlines and the contours of the vertical velocities of the ballistic and collision parts of the solutions, denoted by $u_y^{(b)}$ and $u_y^{(c)}$, respectively, as well as the overall solutions are given for $Kn_0 = 0.05$ and 2 in Fig. 9. More specifically, Figs. 9(a) and 9(b) show the ballistic parts and Figs. 9(c) and 9(d) the collision parts, while the overall solutions which are the summation of the two corresponding parts are shown in Figs. 9(e) and 9(f). It is seen that the streamlines of the ballistic parts (Figs. 9(a) and 9(b)) are directed from the boundaries toward the interior of the bulk flow, while the streamlines of the collision parts (Figs. 9(c) and 9(d)) are directed from the interior of the bulk flow toward the walls. These qualitative observations are well expected from the physical point of view since as it has been pointed before, in the ballistic part the walls act as source and the bulk flow as sink, while it is the other way around in the collision part. The streamlines along with the vertical velocities contours clearly indicate when the flow is in the positive or negative direction corresponding to hot-to-cold and cold-to-hot flow, respectively. The summation of these flow fields deduce the overall solutions shown in Figs. 9(e) and 9(f), which are in excellent agreement with the corresponding deterministic ones. It is seen that for $Kn_0 = 0.05$ only the Vortex-type I are present, while for $Kn_0 = 2$ the Vortex-type II are also well developed, with the gas flowing along the lateral walls in the first case from cold-to-hot and in the second one from hot-to-cold.

The streamlines in Fig. 9 may be further analyzed. Starting with $Kn_0 = 2$, where the flow patterns are simpler, the streamlines of the ballistic and collision parts are directed to and originated

TABLE VI. Average heat flux q_{av} departing from the bottom plate of a square enclosure for various Knudsen numbers and various temperature ratios.

	$T_C/T_H = 0.1$		$T_C/T_H = 0.5$		$T_C/T_H = 0.9$	
Kn_0	Shakhov	DSMC	Shakhov	DSMC	Shakhov	DSMC
0.01	1.33(−2)	1.38(−2)	8.55(−3)	8.60(−3)	1.87(−3)	1.80(−3)
0.1	7.20(−2)	7.16(−2)	5.18(−2)	5.32(−2)	1.19(−2)	1.22(−2)
1	1.48(−1)	1.49(−1)	1.23(−1)	1.27(−1)	2.88(−2)	2.94(−2)
10	1.78(−1)	1.79(−1)	1.50(−1)	1.51(−1)	3.47(−2)	3.50(−2)

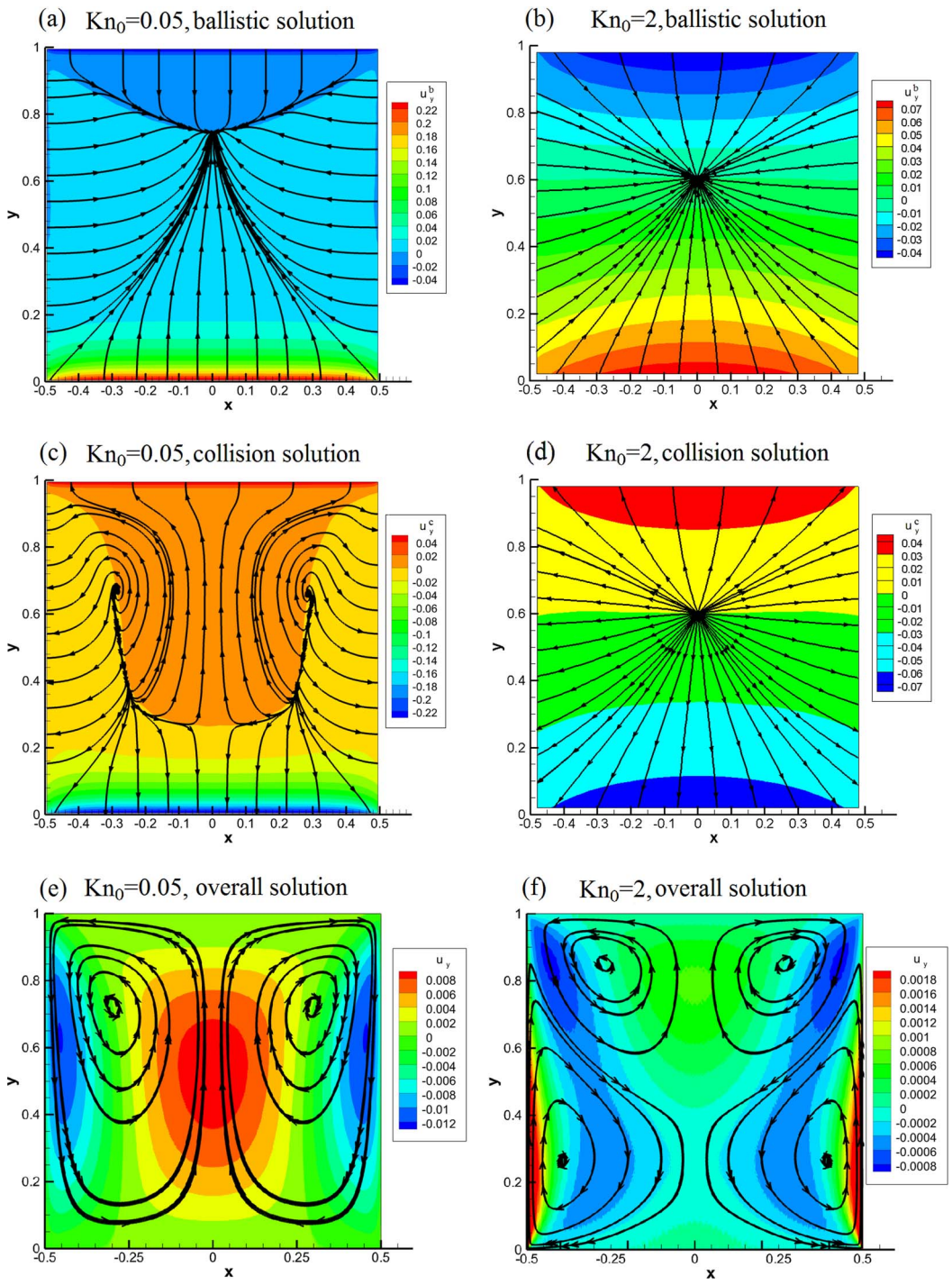

FIG. 9. Streamlines and vertical velocity contours of the ballistic and collision parts as well as of the overall solution in a square enclosure for $Kn_0 = 0.05$ and 2, with $T_C/T_H = 0.1$.

from single points, with total velocity equal to zero. The slight displacement between the two focal points and the small differences in the velocity magnitudes of the collision and ballistic parts, lead to the creation of Vortex-type II, shown in Fig. 9(b). Continuing with $Kn_0 = 0.05$ it is seen that the streamline patterns of the ballistic and collision parts are quite different. The ballistic part has some resemblance with the corresponding one for $Kn_0 = 2$, showing one single point towards which the

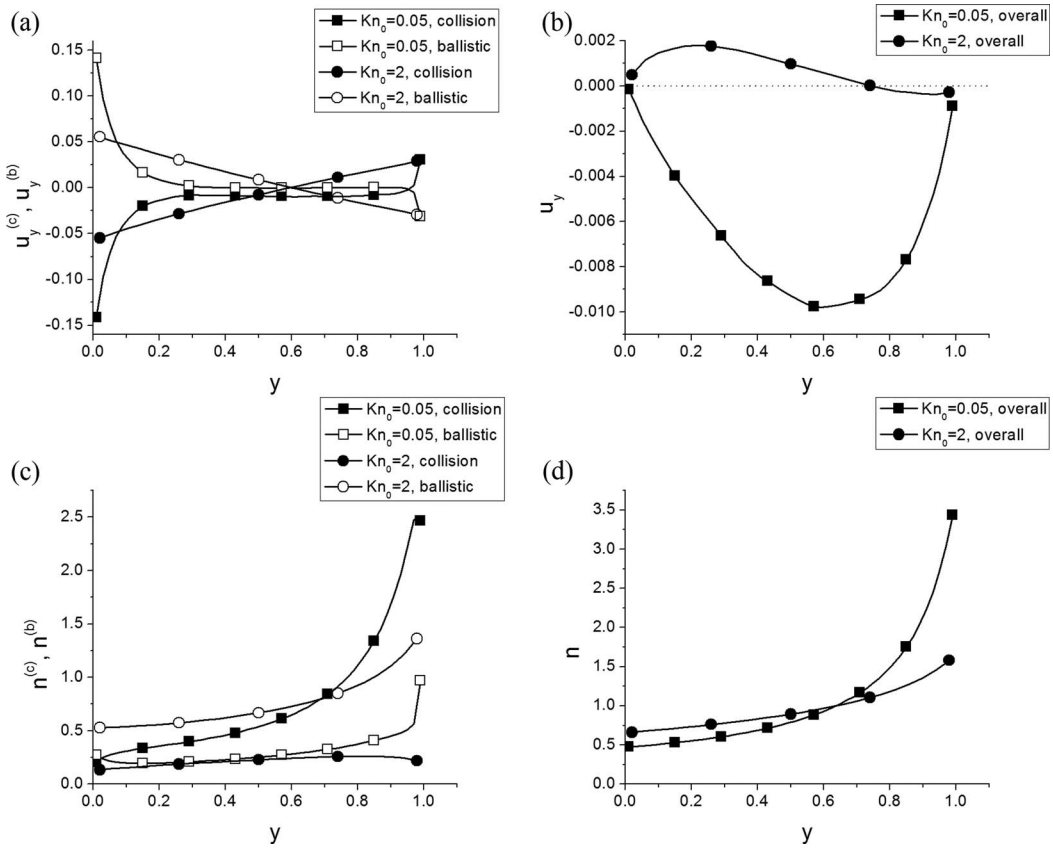

FIG. 10. Tangential velocity and density of the ballistic and collision parts as well as of the overall solution along the lateral walls of a square enclosure for $Kn_0 = 0.05$ and 2, with $T_C/T_H = 0.1$.

streamlines are directed. The collision part however is different indicating two single points from which the streamlines are originated. These points are symmetrically located about $x = 0$ and are centers of two symmetric spiral swirls caused by flow vorticity at this low Knudsen number. Also, at some extent streamlines are concentrated along a curve where the vertical velocities are zero. In addition, there is one point along $x = 0$ where the total velocity is zero and this point is transformed to a saddle point separating the streamline patterns into two branches directed to the hot and cold walls. The slope of the streamlines with respect to the vertical walls is another important element in the present analysis. It is seen that at $Kn_0 = 0.05$ the negative slope of the streamlines of the collision part is larger than the positive slope of the streamlines of the ballistic part and this is a clear sign for a cold-to-hot gas motion along the vertical walls. At $Kn_0 = 2$ the two slopes are about the same with the ballistic one appearing to be larger, which is an indication for a hot-to-cold gas motion.

A more detailed view of the flow along the lateral walls is presented in Fig. 10, where the tangential velocities and number densities are presented. In Fig. 10(a) the tangential velocities of the ballistic and collision parts, $u_y^{(b)}$ and $u_y^{(c)}$, respectively, are plotted along $y \in [0, 1]$ for $Kn_0 = 0.05$ and 2, while the corresponding overall tangential velocities u_y are given in Fig. 10(b). It is seen in Fig. 10(a), that for $Kn_0 = 0.05$, the tangential velocities $u_y^{(b)}$ and $u_y^{(c)}$ are positive and negative, respectively, along almost the whole length of the side walls and only very close to the top corners ($y = 1$) their signs are interchanged. In parallel, the overall tangential velocity u_y, in Fig. 10(b), is negative.

In the case of $Kn_0 = 2$, the tangential velocities $u_y^{(b)}$ and $u_y^{(c)}$ in Fig. 10(a), are positive and negative, respectively, up to about $y = 0.65$ and then their signs are interchanged. The overall velocity u_y, in Fig. 10(b), is positive up to about $y = 0.7$ and then its value becomes negative taking

very small values close to zero. From the above it is deduced that the negative or positive values of u_y, corresponding to cold-to-hot or hot-to-cold flow along the walls depends on which part of the solution, either the ballistic or the collision part prevails with respect to the other. At $Kn_0 = 0.05$ the contribution of the collision part is more significant and only the Vortex-type I flow is observed, while at $Kn_0 = 2$ the magnitude of the ballistic part has been increased and becomes respectively more significant and therefore the Vortex-type II flow shows up.

These arguments are also supported by the ballistic and collision number density profiles denoted by $n^{(b)}$ and $n^{(c)}$, in Fig. 10(c). It is seen that along the walls for $Kn_0 = 0.05$, $n^{(b)} < n^{(c)}$ and for $Kn_0 = 2$, $n^{(b)} > n^{(c)}$, which also indicate that in the overall solution the contribution of the collision part dominates at small Knudsen numbers, while at large Knudsen numbers the contribution of the ballistic part becomes more significant. In Fig. 10(d) the overall density profiles n, computed as the summations of the two parts are provided for $Kn_0 = 0.05$ and 2.

Based on both Figs. 9 and 10 and the previous discussion some more general comments on the ballistic and collision contributions in the overall solution may be stated. In the free molecular limit, the flow is perfectly balanced by pressure and temperature distributions and both collision and ballistic velocities are equal to zero. Increasing the gas density and respectively decreasing the Knudsen number, collisions between molecules destroy this balance and from thermodynamic viewpoint, the gas reaction is a weak motion in the enclosure with streamline patterns depending on the Knudsen number, the wall temperature distribution, and the enclosure geometry. At very large Knudsen numbers, the ballistic part is dominating. At moderate values there is interplay between the ballistic and collision parts and the behavior of the overall solution is very subtle particularly in the transition regime. Finally, at very small Knudsen numbers the collision part is dominating. In this latter case, the classic thermal creep theory works and predicts correctly the cold-to-hot direction of the streamlines along the vertical walls. As the Knudsen number increases the impact of the ballistic part also increases and the convective vortices start to rotate in the hot-to-cold direction along the lateral walls.

VI. CONCLUDING REMARKS

The thermally induced rarefied gas flow in a rectangular enclosure with non-isothermal walls is investigated in terms of the three parameters characterizing the flow, namely, the reference Knudsen number, the temperature ratio of the top over the bottom plates, and the aspect ratio of the enclosure. Both deterministic and stochastic simulations have been performed based on the numerical solution of the Shakhov kinetic equation and the DSMC method, respectively. Results have been obtained for enclosures with various aspect ratios in the whole range of the Knudsen number and for small, moderate, and large temperature differences.

Confirming previous results in similar non-isothermal set-ups, it has been found that in the vicinity of the lateral walls the gas is not necessarily going from cold-to-hot. Actually, even for relatively small Knudsen numbers in the slip or early transition regime a hot-to-cold flow along the non-isothermal side walls is observed, which is enhanced as the Knudsen number and the temperature difference are increased. The cavity aspect ratio is also an important factor and the hot-to-cold flow is becoming more dominant as the depth compared to the width of the cavity is increased. The effect of these parameters on the flow configuration and bulk quantities has been thoroughly examined. Furthermore, the introduced novel decomposition of the DSMC solution into the ballistic and collision parts illuminates, at the particle level, important details of the flow. It has been found that at small Knudsen numbers the collision part dominates and the classic thermal creep theory works, while at large Knudsen numbers the ballistic part prevails and then the gas along the wall flows from hot-to-cold.

It is believed that the present research work has both scientific interest and technological impact and it is hoped to support the design and optimization of devices operating far from local equilibrium. Also, the introduced solution decomposition is rather universal and can be applied to any rarefied gas flow in the transition regime. The theoretical background of the decomposition and its detailed implementation in the DSMC algorithm will be described in a future work.

ACKNOWLEDGMENTS

This research obtained financial support from the Association EURATOM/Hellenic Republic, the EFDA/GOT program VACU-TEC, and the European Community's Seventh Framework programme (FP7/2007-2013) under Grant No. 215504. Also, S.S. would like to acknowledge the partial support provided by the Bulgarian NSF under Grant No. DCVP 02/1-2009.

[1] H. A. Stone, A. D. Stroock, and A. Ajdari, "Engineering flows in small devices: Microfluidics toward a lab-on-a-chip," Annu. Rev. Fluid Mech. **36**, 381–411 (2004).
[2] H. A. Yang, M. C. Wu, and W. L. Fang, "Localized induction heating solder bonding for wafer level MEMS packaging," J. Micromech. Microeng. **15**, 394–399 (2005).
[3] H. Liu, M. Wang, J. Wang, G. Zhang, H. Liao, R. Huang, and X. Zhang, "Monte Carlo simulations of gas flow and heat transfer in vacuum packaged MEMS devices," Appl. Therm. Eng. **27**, 323–329 (2007).
[4] Y. Sone, Y. Waniguchi, K. Aoki, and S. Takata, "One-way flow of a rarefied gas induced in a channel with a periodic temperature distribution," Phys. Fluids **8**(8), 2227–2235 (1996).
[5] A. Alexeenko, S. Gimelshein, E. Muntz, and A. Ketsdever, "Kinetic modeling of temperature driven flows in short microchannels," Int. J. Therm. Sci. **45**, 1045–1051 (2006).
[6] A. Ketsdever, N. Gimelshein, S. Gimelshein, and N. Selden, "Radiometric phenomena: From the 19th to the 21st century," Vacuum **86**, 1644–1662 (2012).
[7] M. Vargas, M. Wüest, and S. Stefanov, "Monte Carlo analysis of thermal transpiration effects in capacitance diaphragm gauges with helicoidal baffle system," J. Phys.: Conf. Ser. **362**, 012013 (2012).
[8] K. Aoki, S. Takata, H. Aikawa, and F. Golse, "A rarefied gas flow caused by a discontinuous wall temperature," Phys. Fluids **13**(9), 2645–2661 (2001).
[9] S. Stefanov, V. Roussinov, and C. Cercignani, "Rayleigh-Benard flow of a rarefied gas and its attractors. II. Chaotic and periodic convective regimes," Phys. Fluids **14**(7), 2270–2288 (2002).
[10] S. Naris and D. Valougeorgis, "Gas flow in a grooved channel due to pressure and temperature gradients," in *Proceedings of ASME 4th International Conference on Nanochannels, Microchannels, and Minichannels, Limerick, Ireland, Paper No. ICNMMM2006-96225 June 19-21, 2006* (ASME, New York, 2006).
[11] Y. Sone, "Comment on "Heat transfer in vacuum packaged microelectromechanical system devices" [Phys. Fluids **20**, 017103 (2008)]," Phys. Fluids **21**, 119101 (2009).
[12] A. Mohammadzadeh, E. Roohi, H. Niazmand, S. Stefanov, and R. S. Myong, "Thermal and second-law analysis of a micro- or nanocavity using direct-simulation Monte Carlo," Phys. Rev. E **85**, 056305 (2012).
[13] N. D. Masters and W. Ye, "Octant flux splitting information preservation DSMC method for thermally driven flows," J. Comput. Phys. **226**, 2044–2062 (2007).
[14] A. Rana, M. Torrilhon, and H. Struchtrup, "Heat transfer in micro devices packaged in partial vacuum," J. Phys.: Conf. Ser. **362**, 012034 (2012).
[15] J. C. Huang, K. Xu, and P. Yu, "A unified gas-kinetic scheme for continuum and rarefied flows III: Microflow simulations," Commun. Comput. Phys. **14**(5), 1147–1173 (2013).
[16] Y. Sone, *Kinetic Theory and Fluid Dynamics* (Birkhäuser, Boston, 2002).
[17] H. Struchtrup and P. Taheri, "Macroscopic transport models for rarefied gas flows: A brief review," IMA J. Appl. Math. **76**(5), 672–697 (2011).
[18] C. Cercignani, *The Boltzmann Equation and its Applications* (Springer, New York, 1988).
[19] G. A. Bird, *Molecular Gas Dynamics and the Direct Simulation of Gas Flows* (Clarendon, Oxford, 1994).
[20] Y. Sone, *Molecular Gas Dynamics: Theory, Techniques and Applications* (Birkhäuser, Boston, 2007).
[21] D. H. Papadopoulos and D. E. Rosner, "Enclosure gas flows driven by non-isothermal walls," Phys. Fluids **7**(11), 2535–2537 (1995).
[22] S. Kosuge, K. Aoki, S. Takata, R. Hattori, and D. Sakai, "Steady flows of highly rarefied gas induced by nonuniform wall temperature," Phys. Fluids **23**, 030603 (2011).
[23] C. Cercignani and M. Lampis, "Kinetic models for gas-surface interactions," Transp. Theory Stat. Phys. **1**, 101–114 (1971).
[24] R. G. Lord, "Some extensions to the Cercignani-Lampis gas-surface scattering kernel," Phys. Fluids A **3**, 706–710 (1991).
[25] A. S. Rana, M. Torrilhon, and H. Struchtrup, "A robust numerical method for the R13 equations of rarefied gas dynamics: Application to lid driven cavity," J. Comput. Phys. **236**, 169–186 (2013).
[26] K. Xu and J. C. Huang, "A unified gas-kinetic scheme for continuum and rarefied flows," J. Comput. Phys. **229**, 7747–7764 (2010).
[27] E. M. Shakhov, "Generalization of the Krook kinetic relaxation equation," Fluid Dyn. **3**(5), 95–96 (1968).
[28] E. M. Shakhov, "Kinetic model equations and numerical results," in *Proceedings of 14th International Symposium on Rarefied Gas Dynamics* (University of Tokyo Press, 1984), pp. 137–148.
[29] M. H. Vargas, "Modeling and simulation of heat transfer and thermal phenomena in micro gas flows," Ph.D. thesis (Institute of Mechanics, Bulgarian Academy of Sciences, 2012).
[30] I. Graur and A. Ph. Polikarpov, "Comparison of different kinetic models for the heat transfer problem," Heat Mass Transfer **46**, 237–244 (2009).
[31] V. A. Titarev, "Rarefied gas flow in a planar channel caused by arbitrary pressure and temperature drops," Int. J. Heat Mass Transfer **55**(21–22), 5916–5930 (2012).
[32] V. A. Titarev and E. M. Shakhov, "Computational study of a rarefied gas flow through a long circular pipe into vacuum," Vacuum **86**(11), 1709–1716 (2012).
[33] V. A. Titarev, E. M. Shakhov, and S. V. Utyuzhnikov, "Rarefied gas flow through a diverging conical pipe into vacuum," Vacuum **101**, 10–17 (2014).

[34] V. A. Titarev, M. Dumbser, and S. V. Utyuzhnikov, "Construction and comparison of parallel implicit kinetic solvers in three spatial dimensions," J. Comput. Phys. **256**, 17–33 (2014).
[35] S. Pantazis and D. Valougeorgis, "Non-linear heat transfer through rarefied gases between coaxial cylindrical surfaces at different temperatures," Eur. J. Mech. B. Fluids **29**, 494–509 (2010).
[36] S. Misdanitis, S. Pantazis, and D. Valougeorgis, "Pressure driven rarefied gas flow through a slit and an orifice," Vacuum **86**, 1701–1708 (2012).
[37] S. Pantazis, S. Naris, C. Tantos, D. Valougeorgis, J. Andre, F. Millet, and J. P. Perin, "Nonlinear vacuum gas flow through a short tube due to pressure and temperature gradients," Fusion Eng. Des. **88**, 2384–2387 (2013).
[38] S. Stefanov, P. Gospodinov, and C. Cercignani, "Monte Carlo simulation and Navier-Stokes finite difference calculation of unsteady-state rarefied gas flows," Phys. Fluids **10**, 289–300 (1998).
[39] S. K. Stefanov, "On DSMC calculations of rarefied gas flows with small number of particles in cells," SIAM J. Sci. Comput. **33**(2), 677–702 (2011).
[40] Y. Sone and T. Takata, "Discontinuity of the velocity distribution function in a rarefied gas around a convex body and the s layer at the bottom of the Knudsen layer," Transp. Theory Stat. Phys. **21**, 501–530 (1992).
[41] K. Aoki, C. Bardos, C. Dogbe, and F. Golse, "A note on the propagation of boundary induced discontinuities in kinetic theory," Math. Models Methods Appl. Sci. **11**(9), 1581–1595 (2001).
[42] S. Naris and D. Valougeorgis, "The driven cavity flow over the whole range of the Knudsen number," Phys. Fluids **17**(9), 097106 (2005).